CIRP Annals - Manufacturing Technology 68 (2019) 451–454

Contents lists available at ScienceDirect

CIRP Annals - Manufacturing Technology

journal homepage: http://ees.elsevier.com/cirp/default.asp

Machine learning-based image processing for on-line defect recognition in additive manufacturing

Alessandra Caggiano [a,b,*], Jianjing Zhang [c], Vittorio Alfieri [d], Fabrizia Caiazzo [d], Robert Gao (1)[c], Roberto Teti (1)[b,e]

[a] Department of Industrial Engineering, University of Naples Federico II, Naples, Italy
[b] Fraunhofer Joint Laboratory of Excellence on Advanced Production Technology (Fh-J_LEAPT UniNaples), Naples, Italy
[c] Department of Mechanical and Aerospace Engineering, Case Western Reserve University, Cleveland, OH, USA
[d] Department of Industrial Engineering, University of Salerno, Fisciano, SA, Italy
[e] Department of Chemical, Materials and Industrial Production Engineering, University of Naples Federico II, Naples, Italy

ARTICLE INFO

Keywords:
Machine learning
Additive manufacturing
Fault recognition

ABSTRACT

A machine learning approach for on-line fault recognition via automatic image processing is developed to timely identify material defects due to process non-conformities in Selective Laser Melting (SLM) of metal powders. In-process images acquired during the layer-by-layer SLM processing are analyzed via a bi-stream Deep Convolutional Neural Network-based model, and the recognition of SLM defective condition-related pattern is achieved by automated image feature learning and feature fusion. Experimental evaluations confirmed the effectiveness of the machine learning method for on-line detection of defects due to process non-conformities, providing the basis for adaptive SLM process control and part quality assurance.

1. Introduction

In recent years, metal additive manufacturing (AM) processes are capturing increasing interest from industry, in particular from the medical and aerospace sectors attracted by the possibility to realize innovative shapes, complex features, lightweight structures and by the low material consumption offered by AM [1–3].

In particular, laser-based AM technologies such as Selective Laser Melting (SLM) proved a high potential for industrial applications due to several advantages (like higher feature resolution and accuracy) compared to other freeform fabrication techniques [1,4,5]. SLM is based on laser irradiation of a pre-laid bed of metal powder: a thin metal powder layer is laid on a plane substrate by a deposition system and a laser beam scans the powder layer along a preset path to locally melt the powder and build a slice of the part. After layer scanning, the plane substrate is moved downwards, a new metal powder layer is deposited, and laser scanning is repeated to construct the next slice. Inert gas such as N or Ar is employed to prevent surface oxidization [4,6].

The main barriers to the widespread adoption of the SLM technology are related to the need to improve the part quality and repeatability [7,8]. Indeed, SLM is of special interest for precision metal AM requiring avoidance of non-conformities and defects. However, defect presence is still too high compared to traditional manufacturing technologies and several categories of defects can occur during the layer-by-layer part construction [3]. Depending on process conditions, part quality issues include lack of fusion, residual porosity, balling (metal droplets), spatter, etc. [9,10]. Most often, defects cannot be eliminated by post-processing: thus, it is essential to improve the quality of the SLM product at part building stage. This is a challenging goal as many parameters affect the part quality, making it difficult to define the optimal process conditions, and modelling is not fully developed for this process [11].

As a result, research on in-process sensor monitoring of SLM has attracted attention in the manufacturing community [7]. As the SLM part is built layer-by-layer, the characteristics of each layer affect the final part quality, and layer-wise in-process sensing can be employed to extract condition-related features and help on-line recognition of defects induced by improper process conditions. In the literature, diverse SLM process monitoring approaches have been developed based on non-contact temperature measurements or imaging in the visible range with the main aim to characterize the melt-pool, an important indicator of the SLM process [3,7,11]. However, expensive high frame-rate imaging systems are required to effectively track the melt-pool movement, and the high-speed data stream makes timely data analysis hard. As an alternative, SLM process evaluation can be performed based on the properties of single powder layers (thin layers of loose powder deposited by the recoating system) and part slices (part layers consolidated after laser scanning) [3]. Some examples of this approach have been reported, e.g. using a high-resolution camera to capture the images of consolidated layers for quality evaluation [12]. However, image analysis was carried out manually based on empirical knowledge, limiting the efficacy for on-line process monitoring.

* Corresponding author at: Department of Industrial Engineering, University of Naples Federico II, Naples, Italy.
E-mail address: alessandra.caggiano@unina.it (A. Caggiano).

https://doi.org/10.1016/j.cirp.2019.03.021
0007-8506/

In-process data analytics in this field can be effectively supported by machine learning techniques to discover complex patterns in the data for recognition and classification. Machine learning methods like Histogram of Oriented Gradients (HoG) or visual words have long been explored for automated image analysis [13]. However, feature extraction using these methods is unsupervised, limiting the features relevance for the specific recognition task.

In this framework, a machine learning approach based on a Deep Convolutional Neural Network (DCNN) is developed in this work to identify defects due to SLM process non-conformities through automatic image processing. Inspired by the hierarchical neural structure in visual cortex, DCNN is able to automatically extract multi-level image features and discover the embedded patterns that are most relevant to the given problem via supervised learning [14]. The DCNN efficacy was proved in various scenarios of manufacturing (inspection, motion recognition, etc.) [15–17].

In this work, a bi-stream DCNN structure is developed to analyze both SLM powder layers and part slices images for recognition of defects induced by improper SLM process conditions. The surface pattern deviation in the part slices due to the changing process conditions could affect the next powder layer surface pattern, and the irregularity in the powder layer could in turn impact the surface pattern of the subsequent part slice. The bi-stream DCNN is able to fuse the patterns discovered from both layers images to jointly classify the defects due to SLM process non-conformities.

To experimentally evaluate the efficacy of the bi-stream DCNN approach, an SLM testing campaign was carried out by changing the levels of the governing SLM process parameters to generate part structural defects, such as trace discontinuity, protruding sector edges and layer boundary, insufficient layer densification. In-process images of single powder layers and part slices under diverse process conditions were captured and jointly fed to the bi-stream DCNN during network training, allowing the model to establish the correspondence between the layer-wise image surface patterns and the structural defects induced by improper process conditions, providing the basis for part quality assurance.

2. DCNN-based machine learning for SLM process monitoring

The Deep Convolutional Neural Network (DCNN) is a deep neural network architecture specialized in image processing and pattern recognition. The DCNN hierarchical structure allows multi-level image features to be extracted to achieve accurate pattern discovery. In this study, the sequential nature of the SLM process, with the powder layer and part slice alternately produced through powder recoating and laser scanning, implies that defects due to improper process conditions can be manifested in the surface patterns of both layers. To effectively analyze the information embedded in both images for defect-related pattern discovery, a bi-stream DCNN structure was developed, as illustrated in Fig. 1.

2.1. Bi-stream DCNN architecture

Each stream of the bi-stream DCNN consists of a series of convolutional layers. The features of the input image are extracted through the kernel-based convolution and non-linear activation. Mathematically, feature extraction is expressed as:

$$z_j^l = \phi\left(b_j^l + \sum_{i=1}^{M} z_i^{l-1} \cdot w_{ij}^{l-1}\right) \quad (1)$$

where z_j^l is the *jth* feature in the *lth* convolutional layer, b_j^l is the corresponding bias term, M is the kernel size, w_{ij}^{l-1} denotes the kernel weight connecting the *ith* point in the $(l-1)$th layer and the *jth* feature in the *lth* layer, $\phi(.)$ is the non-linear activation function.

By traversing the image, the kernel is able to generate a feature map corresponding to the entire image. Multiple feature maps of interest can be extracted by simultaneously incorporating multiple kernels. As the feature extraction process propagates in the network, the hierarchically arranged convolutional layers gradually assemble lower-level features into higher-level features. The comprehensive feature extraction and selection over successive convolutional layers is essential for the network to discover the layer surface patterns that can be accurately related to the SLM defects due to improper process conditions.

In each convolutional layer, feature extraction is accompanied by the loss of information. In standard CNN, the higher layer can only see the extracted features from the preceding layer, without access to the original input image or the lower-level features [14]. Therefore, as the extraction process propagates into deeper layers, the loss is accumulated and reduces the information richness for higher level of feature extraction in the standard CNN. In the bi-stream DCNN, skip connections are incorporated among the input image and the convolutional layers. The skip connection allows the higher layers to gain full access to the input image and the preceding multi-level image features and therefore, improving the information richness to achieve accurate higher-level feature extraction for pattern recognition. Specifically, the input image and lower-level feature maps are first duplicated and sent to the higher convolutional layers, as indicated by the dash-dot lines in Fig. 1. Then, they are stacked with the high-level feature maps to jointly participate in the convolution for following feature extraction. The fully connected layers, fed with the feature maps from the last convolutional layer in both streams, fuse the highest-level features extracted from both images. A classification layer takes the fused feature and classifies the defective condition-related image pattern via a softmax function. In a model to recognize n diverse patterns, for a fused feature input $\boldsymbol{x} = [x_1, x_2, \ldots, x_n]$, the softmax function is $p(\mathbf{x}) = [e^{x_1}, e^{x_2}, \ldots, e^{x_n}] / \sum_{i=1}^{n} e^{x_i}$. The *ith* entry in $p(\boldsymbol{x})$ is the probability that the input image pattern corresponds to the *ith* defective condition. Mathematically, $p(\boldsymbol{x})$ is a predicted discrete probability distribution among all candidate SLM defective condition-related patterns for an input image. The classification layer selects the defective condition with the highest probability.

2.2. Bi-stream DCNN training

The aim of bi-stream DCNN training is to find the optimal convolution kernels for SLM defective condition-related pattern recognition. The minimization of the prediction error represents the optimality criterion. In this study, the prediction error is formulated as $H(p,q) = -\sum_x q(x) \log p(x)$, or cross-entropy error, where $p(x)$ is the classification from the softmax function corresponding to an input image and $q(x)$ is the ground truth

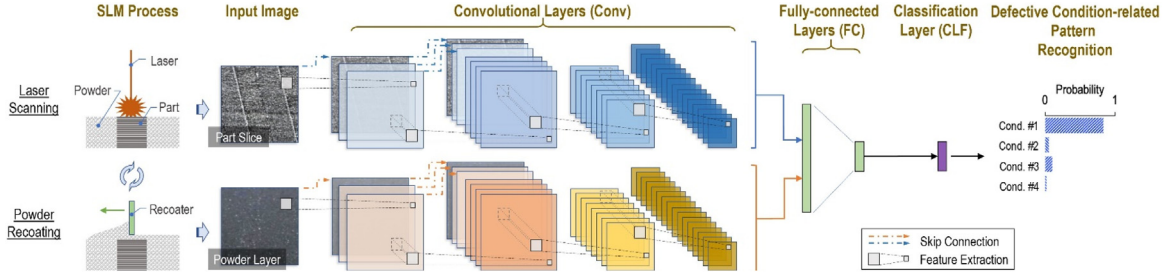

Fig. 1. Bi-stream DCNN for recognition of defects induced by improper SLM process conditions.

label of that image. The training is realized by recursively updating the kernel weights using the training images. The weights update at each layer is guided by the gradient of the prediction error backpropagated to that layer, that indicates the direction of weight adjustment which allows the fastest decrease of prediction error.

Similar to the loss of information during the forward propagation in standard CNN, loss of information also occurs when the gradient of the prediction error backpropagates in the network. The available gradient is gradually reduced as it passes through more layers. This is known as the vanishing gradient problem [14].

Therefore, the benefit of skip connection can be extended to the training process of bi-stream DCNN, allowing lower level layers to access the gradient in the higher layer for more effective weights update, as the loss of gradient in higher layers is relatively small.

3. Experimental evaluation

The efficacy of the bi-stream DCNN for recognition of defective conditions due to process non-conformities was experimentally evaluated via an SLM testing campaign carried out on a EOS 270 system with a Yb fibre-based laser source. Pre-alloyed Inconel 718 powder with 20 μm mean grain size widely employed in aerospace, was used. The final part is a disc of 40 mm diameter and 20 mm height. Each part slice is split into parallel stripe sectors with 0.12 mm overlapping, in which the laser scan traces, transverse to the sector axis, are spaced with preset hatch value (Fig. 2). The scan direction is rotated by 67° between successive slices. 20 μm thick powder layers are deposited by a brush recoater at 80 mm/s. Inert Ar atmosphere was provided with residual O_2 content <0.1%.

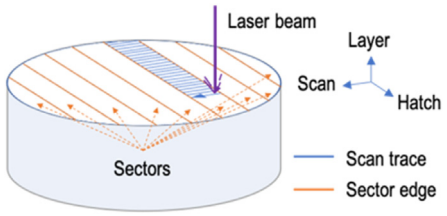

Fig. 2. Sectors, scan and hatch spacing direction in the experiments.

Four tests under different process conditions were executed by varying the SLM process parameters (Table 1). Test A represents the standard process conditions as per previous studies on SLM of the same alloy [5]. For the other conditions, the levels of the process governing factors were changed to verify part fault generation due to process conditions with different levels of delivered energy per unit volume, E_v (Table 1), which is the most relevant input parameter affecting part quality, given by [9,10]:

$$E_v = \frac{P}{h \cdot u \cdot t} \quad (2)$$

Table 1
Different process conditions employed in the four experimental tests.

Test	P [W]	u [mm/s]	h [mm]	E_v [J/mm^3]
A (standard)	195	1200	0.09	90
B	155	1200	0.11	60
C	195	400	0.05	480
D	100	2400	0.09	23

where P is the operating laser power, h the hatch spacing between laser traces, u the laser beam scanning speed, t the layer thickness.

To acquire images during the layer-by-layer SLM process, a 24.2 megapixel single-lens reflex digital camera with 18–105 mm f/3.5–5.6 G ED VR lens (with 5.8 × zoom) was used. The camera was mounted outside the building chamber in off-axial configuration with 35° angle-of-view with respect to the area of interest. Videos of the entire SLM tests were acquired and processed to extract, layer-by-layer, 2 images: one after powder deposition (powder layer) and one after SLM of the powder layer (part slice). A cross-test comparison of part slice images is shown in the left column of Fig. 3. These images and the matching powder layer images are fed into the bi-stream DCNN. Off-line microscope images were taken to verify the microstructural details and confirm the defect types induced by diverse process conditions. The white rectangle in part slice images (left column) corresponds to the microscopic image in the right column, which highlights the sector edges.

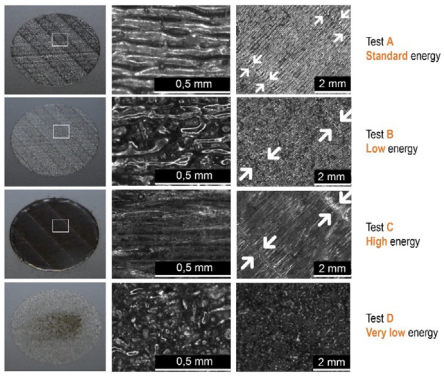

Fig. 3. Left column: part slice images (input to DCNN); white rectangles correspond to the sector edge views. Middle column: microscope view of sector region. Right column: microscope view of sector edges (arrows).

The within-sector regions are shown in the microscopic images displayed in the middle column. From Fig. 3, it can be seen that for test A, under standard process conditions, the scan trace is uniform and continuous. When E_v is reduced in test B, the scan traces become fragmented and several discontinuities appear. When E_v is increased in test C, a higher level of remelting and resolidification occurs, leading to less discernable scan traces and more prominent sector edges and layer boundary which are a major source of delamination defect in the final part. Non-densification occurred in test D due to very low E_v, where powder clumps, sintered but not completely melted, are visible. Moreover, sector edges are not visible, hence no arrow is shown in the relative sector edge image.

To train the bi-stream DCNN, images from 150 powder layers and related 150 part slices from each test are collected. 70% of the images (840) are used for network training while the remaining 30% (360) are used for testing. Five random training/testing splits are used to assess model robustness. All input images are cropped to 160 px × 160 px size around the cross-sectional center. Table 2 lists the network parameters for the bi-stream DCNN. Stride is the step size with which a kernel traverses the image. A stride of 2 in the last 2 layers reduces the network parameters by a factor of 16. Kernel size is 3 px × 3 px for all layers and learning rate is 0.001.

Table 2
Parameters of the bi-stream DCNN.

Layer	Size (pixels)	#Feature maps	Stride	Activation
Conv #1	160 × 160	4	1	ReLU
Conv #2	160 × 160	8	1	ReLU
Conv #3	80 × 80	16	2	ReLU
Conv #4	40 × 40	32	2	ReLU
FC	64	n/a	n/a	ReLU
CLF	4	n/a	n/a	Softmax

Fig. 4 shows a pair of classification accuracy curves from training and testing: they are closely aligned with a Pearson correlation coefficient of 0.996, indicating no overfitting in network training. The impact of skip connections on computational complexity was also evaluated. It was found that the network with skip connections took 10 less iterations on average to achieve the same classification accuracy than the one without skip connections. Representative feature maps from the final convolutional layer at different classification accuracy, 50%, 75% and 100%, are plotted in Fig. 5, reflecting the progression of high-level feature generation.

An increase in pixel intensity indicates the increase of neural response in the feature map. The raw input images from each test

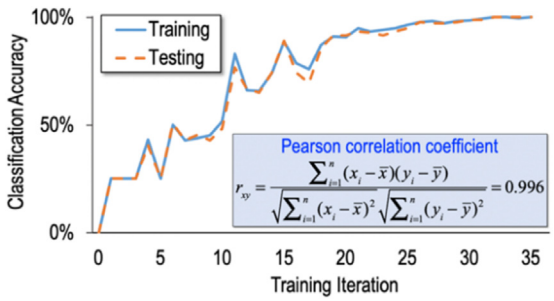

Fig. 4. Classification accuracy curves during the training process.

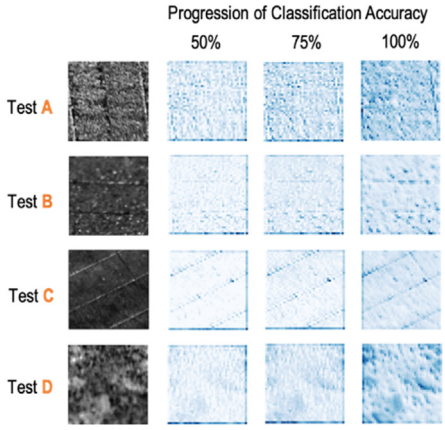

Fig. 5. Feature map progression in convolutional layers during training.

are shown on the left as reference. It can be seen that, as the training progresses, the neural response in the feature map gradually converges to the prominent characteristics observed in the captured part slice images. E.g., for the input images of tests A to C, at 50% classification accuracy, the sector overlapping edges are barely captured in the feature map. As the training continues, the neural response starts to better highlight the edges in the feature map and the classification accuracy improves. For test D images, as the classification accuracy improves, the light and dark spots become more discernable. This means that the underlying network parameters (e.g. kernel weights), initialized randomly, gradually learn during training and converge to more accurately describe the input images and improve the classification accuracy.

The performance of the developed bi-stream DCNN was compared to HoG and visual words, two commonly reported image processing techniques [13]. Both methods characterize an image by features describing regional patterns. HoG exploits the gradient of pixel intensity for object edge detection, as the pixels on diverse edge sides have contrasting intensities. Thus, the objects in the region are inferred by the distribution of gradient orientations (e.g. while a square only has horizontal and vertical gradients, a circle has evenly distributed gradients in all orientations). The feature vector describing the entire image is then assembled using all regional distributions. In visual words, the regional distribution of gradient orientations obtained from all the images are first clustered into high-level gradient pattern representations (i.e. visual words). The final feature vector of each image is a histogram counting the occurrences of each visual word in that image [13]. In both methods, a support vector machine classifier is trained on the feature vectors for defective condition recognition. As shown in Fig. 6, DCNN achieved a mean defective condition-related image pattern recognition accuracy of 99.4% across 5 random tests, as compared to 96.5% and 91.2% from HoG and visual words, confirming the higher effectiveness of the developed method in recognizing defects induced by improper SLM process conditions.

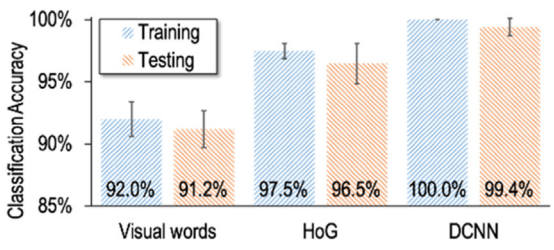

Fig. 6. Performance comparison among DCNN, HoG and visual words.

4. Conclusions

With the aim to improve process monitoring and quality control for Selective Laser Melting (SLM), a machine learning model based on bi-stream Deep Convolutional Neural Network (DCNN) was developed to characterize layer-wise images of the SLM process for on-line identification of defects induced by process non-conformities. An SLM experimental evaluation was carried out demonstrating that the bi-stream DCNN was effectively reinforced by the fusion of information from in-process images of SLM powder layers and part slices. The developed machine learning method achieved an accuracy as high as 99.4% in SLM defective conditions recognition. This on-line fault detection can be applied for adaptive SLM process control and part quality assurance.

Acknowledgements

Constructive input from Dr. Peng Wang at Case Western Reserve University to improve the paper is sincerely appreciated.

The Fraunhofer BioMANU II project is gratefully acknowledged for its inspiration and support of this paper.

References

[1] Schmidt M, Merklein M, Bourell D, Dimitrov D, Hausotte T, Wegener K, Overmeyer L, Vollertsen F, Levy GN (2017) Laser Based Additive Manufacturing in Industry and Academia. *CIRP Annals Manufacturing Technology* 66:561–583.
[2] Kopf R, Gottwald J, Jacob A, Brandt M, Lanza G (2018) Cost-Oriented Planning of Equipment for Selective Laser Melting (SLM) in Production Lines. *CIRP Annals Manufacturing Technology* 67:471–474.
[3] Grasso M, Colosimo BM (2017) Process Defects and in situ Monitoring Methods in Metal Powder Bed Fusion: a Review. *Measurement Science & Technology* 28044005.
[4] Gibson I, Rosen DW, Stucker B (2010) *Additive Manufacturing Technologies*, Springer, New York.
[5] Caiazzo F, Alfieri V, Corrado G, Argenio P (2017) Laser Powder-Bed Fusion of Inconel 718 to Manufacture Turbine Blades. *The International Journal of Advanced Manufacturing Technology* 93:4023–4031.
[6] Brinksmeier E, Levy G, Meyer D, Spiering AB (2010) Surface Integrity of Selective-Laser-Melted Somponents. *CIRP Annals Manufacturing Technology* 59(1):601–606.
[7] Everton SK, Hirsch M, Stravroulakis P, Leach RK, Clare AT (2016) Review of in-situ Process Monitoring and in-situ Metrology for Metal Additive Manufacturing. *Materials & Design* 95:431–445.
[8] Kruth JP, Levy G, Klocke F, Childs THC (2007) Consolidation Phenomena in Laser and Powder-Bed Based Layered Manufacturing. *CIRP Annals Manufacturing Technology* 56(2):730–759.
[9] Cardaropoli F, Alfieri V, Caiazzo F, Sergi V (2012) Dimensional Analysis for the Definition of the Influence of Process Parameters in Selective Laser Melting of Ti–6Al–4V Alloy. *Proceedings of the Institution of Mechanical Engineers Part B Journal of Engineering Manufacture* 226(7):1136–1142.
[10] Andani MT, Dehghani R, Karamooz-Ravari MR, Mirzaeifar R, Ni J (2017) Spatter Formation in Selective Laser Melting Process Using Multi-laser Technology. *Materials & Design* 131:460–469.
[11] Furumoto T, Egashira K, Munekage K, Abe S (2018) Experimental Investigation of Melt Pool Behaviour During Selective Laser Melting by High Speed Imaging. *CIRP Annals Manufacturing Technology* 67:253–256.
[12] Kleszczynski S, Zur Jacobsmühlen J, Sehrt JT, Witt G (2012) Error Detection in Laser Beam Melting Systems by High Resolution Imaging. *International Solid Free Fabrication Symposium*, 975–987.
[13] Li Y, Wang S, Tian Q, Ding X (2015) Feature Representation for Statistical-Learning-Based Object Detection: a Review. *Pattern Recognition* 48(11):Error: FPage (3542) is higher than LPage (3559)!.
[14] Gu J, Wang Z, Kuen J, Ma L, Shahroudy A, Shuai B, Liu T, Wang L, Cai J (2015) Recent Advances in Convolutional Neural Networks. *Pattern Recognition* 77:354–377.
[15] Wang P, Liu H, Wang L, Gao RX (2018) Deep Learning-Based Human Motion Recognition for Predictive Context-aware Human-robot Collaboration. *CIRP Annals Manufacturing Technology* 67(1):17–20.
[16] Wang J, Ma Y, Zhang L, Gao RX, Wu D (2018) Deep Learning for Smart Manufacturing: Methods and Applications. *International Journal of Industrial and Manufacturing Systems Engineering* 48:144–156.
[17] Weimer D, Scholz-Reiter B, Shpitalni M (2016) Design of Deep Convolutional Neural Network Architectures for Automated Feature Extraction in Industrial Inspection. *CIRP Annals Manufacturing Technology* 65(1):417–420.